

# Sampling uncertainties of particle size distributions and derived fluxes

Kelsey M Bisson<sup>1</sup>, Rainer Kiko<sup>2</sup>, David A. Siegel<sup>3</sup>, Lionel Guidi<sup>4</sup>, Marc Picheral<sup>5</sup>, Emmanuel Boss<sup>6</sup>, and B. B. Cael<sup>7</sup>

<sup>1</sup>Oregon State University

<sup>2</sup>GEOMAR Helmholtz Centre for Ocean Research Kiel, Germany

<sup>3</sup>University of California, Santa Barbara

<sup>4</sup>French National Centre for Scientific Research (CNRS)

<sup>5</sup>CNRS/UPMC

<sup>6</sup>School of Marine Sciences, University of Maine, Orono, ME, USA

<sup>7</sup>National Oceanography Centre

November 24, 2022

## Abstract

The Underwater Vision Profiler (UVP) provides abundant in situ data of the marine particle size distribution (PSD) on global scales and has been used for a diversity of applications, but the uncertainty associated with its measurements has not been quantified. Here we use a global compilation of UVP (version 5) observations of the PSD to assess the sampling uncertainty associated with the UVP's sampling characteristics. We model UVP sampling uncertainty using Bayesian Poisson statistics and provide formulae for the uncertainty associated with a given sampling volume and observed particle count. We also model PSD observations using a power law with an exponential cutoff to better match the low concentration associated with rare large particles as seen by the UVP. We use the two shape parameters from this statistical model to describe changes in the PSD shape across latitude band, season, and depth. The UVP sampling uncertainty propagates into an uncertainty for modeled carbon flux exceeding 50%. The statistical model is used to extend the size interval used in a PSD-derived carbon flux model, revealing a high sensitivity of the PSD-derived flux model to the inclusion of small particles (80-128 microns). We close with recommendations on how to revise the carbon flux model, and we provide avenues to address additional uncertainties associated with UVP-derived carbon flux calculations.

# 1            **Sampling uncertainties of particle size distributions and derived fluxes**

2   **K. M. Bisson<sup>1</sup>, R. Kiko<sup>2</sup>, D.A. Siegel<sup>3</sup>, L. Guidi<sup>2</sup>, M. Picheral<sup>2</sup>, Emmanuel Boss<sup>4</sup> and B. B.**  
3   **Cael<sup>5</sup>**

4   <sup>1</sup>Department of Botany and Plant Pathology, Oregon State University, Corvallis, USA

5   <sup>2</sup>Laboratoire d'Océanographie de Villefranche-sur-mer, Sorbonne Université, Villefranche-sur-  
6   mer, France

7   <sup>3</sup>Earth Research Institute and Department of Geography, University of California, Santa  
8   Barbara, Santa Barbara, USA

9   <sup>4</sup>School of Marine Sciences, University of Maine, Orono, Maine 04469, USA

10   <sup>5</sup>National Oceanography Centre, European Way, Southampton, SO143ZH, UK

11  
12   Corresponding author: Kelsey Bisson ([bissonk@oregonstate.edu](mailto:bissonk@oregonstate.edu))

## 13   **Key Points:**

- 14   • We model uncertainty in UVP5-derived PSDs and fluxes via Bayesian Poisson statistics  
15   and a truncated power law distribution.
- 16   • Modeled carbon flux calculations have an uncertainty of ~50% arising from sampling  
17   uncertainty.
- 18   • The carbon flux model is highly sensitive (up to 6-fold differences) to the inclusion of  
19   80-128  $\mu\text{m}$  particles.

## Abstract

The Underwater Vision Profiler (UVP) provides abundant in situ data of the marine particle size distribution (PSD) on global scales and has been used for a diversity of applications, but the uncertainty associated with its measurements has not been quantified. Here we use a global compilation of UVP (version 5) observations of the PSD to assess the sampling uncertainty associated with the UVP's sampling characteristics. We model UVP sampling uncertainty using Bayesian Poisson statistics and provide formulae for the uncertainty associated with a given sampling volume and observed particle count. We also model PSD observations using a power law with an exponential cutoff to better match the low concentration associated with rare large particles as seen by the UVP. We use the two shape parameters from this statistical model to describe changes in the PSD shape across latitude band, season, and depth. The UVP sampling uncertainty propagates into an uncertainty for modeled carbon flux exceeding 50%. The statistical model is used to extend the size interval used in a PSD-derived carbon flux model, revealing a high sensitivity of the PSD-derived flux model to the inclusion of small particles (80-128 microns). We close with recommendations on how to revise the carbon flux model, and we provide avenues to address additional uncertainties associated with UVP-derived carbon flux calculations.

## Plain Language Summary

The size of a particle in the ocean influences its ecological role. Carbon included in bigger sinking particles are thought to be removed from the surface ocean and possibly sequestered from the atmosphere. The Underwater Vision Profiler (UVP) is a camera system that takes pictures of particles from the ocean's surface to depth. The UVP images a small portion of the water column (~1L at the highest frequency), and does not often capture rare large particles thought to be important for carbon storage. We use statistical models to assess the uncertainty in particle concentrations associated with the UVP, and we calculate the uncertainty of sinking carbon calculated from UVP observations. We find a formula for UVP sampling uncertainty that depends on particle counts and sampling volume. The associated sinking carbon rate uncertainty is ~50%. We also model UVP observations using a statistical model that captures rare, large particles better than a commonly used power law. We use this updated PSD model to 1) describe changes in the PSD shape across depth, time, and place, and 2) test how sinking carbon

calculations change when a different size range is used. The sinking carbon relationship is very sensitive to small particles.

## 1 Introduction

In the ocean, an extraordinary range of particle sizes (from  $< 1 \mu\text{m}$  to 30m; including non-living dust particles, detrital matter, bacteria, phytoplankton, zooplankton including salp chains, whales and many others) influence ecosystem structure and function, net primary production, particle sinking, and carbon flux (Sheldon et al., 1972, White et al., 2015, Alldredge and Gotschalk, 1988, Siegel et al., 2014). Over the last decade, bio-optics has enabled the characterization of portions of the particle size distribution (PSD) (Boss et al., 2001, Slade and Boss, 2015, Dall’Olmo et al., 2009, Reynolds et al., 2010, Chase et al., 2020, Stemmann and Boss, 2012, Cael and White 2020, Giering et al., 2020 and refs therein), especially through the advancement of in situ imaging technologies.

In order to use PSD observations in the most meaningful way in analyses and models, the uncertainty associated with the observations must be clearly quantified. In situ observations of the PSD are a function of both the true size structure of the particle assemblage and of the measurement method. In this study we focus on PSD data collected from the Underwater Vision Profiler (UVP, Gorsky et al., 2000, Picheral et al., 2010), which ‘sees’ a narrow size range (60 microns – 20,000 micron capabilities, Lombard et al., 2019) of living and non-living particles which are imaged within a small fraction of the water column (anywhere from 0.28L to 10.5L depending on the UVP version, Guidi et al., 2008). The surface area of pixels containing a particle is converted into an assumed equivalent spherical diameter using instrument specific calibrations (Picheral et al., 2010), no matter how a particle is shaped or oriented (introducing error into the retrieved particle size e.g., Karp-Boss et al., 2007).

Uncertainties in particle detection are propagated downstream into calculations of carbon flux and other applications, which rely on both accurate PSD observations as well as appropriate modeling to convert standing stocks of PSD observations into rates of sinking carbon across the full range of depths and particle types in the ocean. When PSDs are not used directly for calculations of flux or other quantities of interest, PSDs are commonly described with a power law to reflect the rapid decline in particle concentrations with increasing particle size (e.g., Jonasz and Fournier, 2011). However, the power-law exponent estimation is sensitive to the abundance of rare



large particles, and the behavior of power-law distributed quantities (e.g., carbon flux) is sensitive to the exact values of the power-law exponent. In any natural system, a power law is only applicable over a finite size range and this size range must be adequately accounted for. We model PSD observations with a truncated power law rather than a power law to better account for rare instances of large particles observed by in situ instruments. Moreover, a truncated power law distribution has an extra parameter about the particle size range for which power-law behavior holds, which offers more information about the shape of the particle size distribution than a scaling exponent alone.

In this study we quantified the sampling uncertainty associated with UVP observations as well as the error associated with extrapolation to other size classes. As a test of how UVP sampling uncertainties propagate into derived properties, we calculated carbon flux using both observed and modeled UVP particle concentrations over various size intervals. We discuss implications for the 2 retrieved parameters of the truncated power law distribution and we provide recommendations for future flux modeling of the PSD.

## **2 Materials and Methods**

### **2.1 UVP Data**

Profiles of PSD observations used in this study come from Kiko et al., 2021, which synthesized observations from the UVP5 models only (Figure 1A). This dataset underwent very little processing prior to our analysis. All data were already binned to 5m vertical bins, and the reported particle concentrations are within standardized and consistent size bins, starting at 128  $\mu\text{m}$  for this dataset. For each depth we multiplied the particle concentration ( $\# \text{ L}^{-1}$ ) by the sampling volume specific to each depth in order to retrieve  $N(d)$ , or the total number of particles for a reported equivalent diameter size range. The PSD data reported here includes all living and non-living particles, and all data are inter-calibrated according to procedures described in Kiko et al., 2021.

Since its invention, the UVP has undergone design improvements so that its size and sampling speed are compatible with a standard CTD rosette. The UVP5 (Picheral et al., 2010) has an image acquisition frequency varying between about 3 to 20 Hz depending on versions and particle load of the water column (higher loads require more processing time and therefore a lower acquisition frequency). During normal CTD deployments with speeds up to 1 m/s, this

allows imaging of up to 1L/image at the highest frequency of 20Hz and 20L/m on a vertical profile at 1m/s. The surface area of particles is converted from pixel counts (using instrument settings), and the equivalent spherical diameter (ESD) is calculated following  $aa * \text{number\_of\_pixels}^b$  where  $aa$  and  $b$  were determined through calibration casts in the bay of Villefranche. Hereafter any use of the UVP is implied to mean UVP5 in our study.

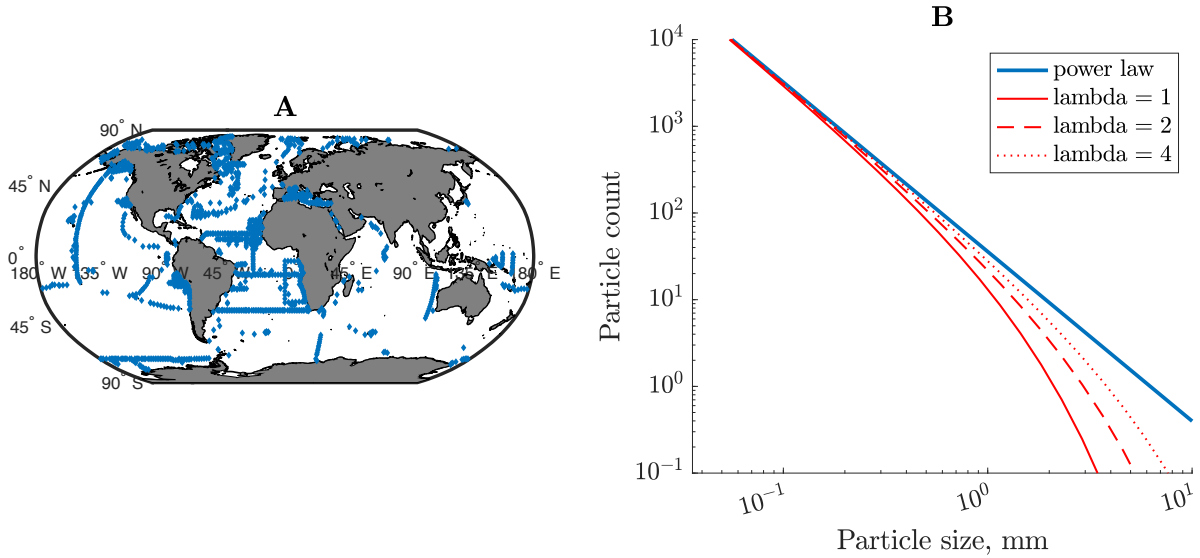


Figure 1. A. Location of UVP5 observations (blue). B. Comparison of a power law (blue) with a power law with an exponential cutoff of various  $\lambda$  values (red lines). All lines share the same  $\alpha$ . The power law is of the form  $N(d) = d^{-\alpha}$  while the truncated power laws follow  $\sim d^{-\alpha} * e^{\frac{-d}{\lambda}}$ .

## 2.2 Extrapolation and sampling uncertainty calculations

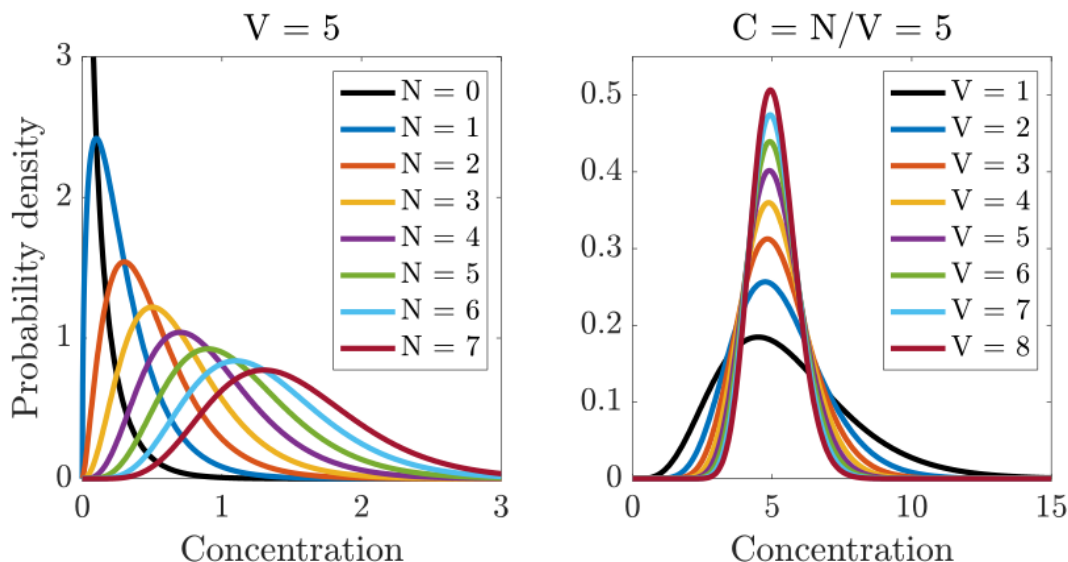
A UVP measurement of the PSD is an estimate of the true particle population in the water column. If a UVP samples  $N$  particles within a range of sizes with average diameter  $d$  in a volume  $V$ , intuitively the best estimate for the concentration of  $d$ -sized particles is  $N/V$ , and the larger  $V$  and/or  $N$  the better an estimate this will be — but what is the uncertainty associated with this estimate, and how does it depend on  $N$  and  $V$ ? How do these uncertainties ultimately propagate into uncertainty in estimated flux? Because particle dis/aggregation is complex, this problem is intractable to quantify perfectly, but may be substantially simplified by assuming Poisson statistics, i.e. that if the true concentration is  $C$ , and a volume  $V$  is being sampled, the likelihood of each particle being sampled is independently  $C \times V$ .

Assuming Poisson statistics, we take a Bayesian approach to finding the best estimate and uncertainty in the true concentration given the measured concentration. The Poisson distribution expresses the probability of a given number of events occurring in a fixed interval of time or space if these events occur independently with a known rate (Haight, 1967). Thus, if the probability of individual particles being sampled by the UVP is independent, and the concentration of particles of mean size  $d$  is some concentration  $C$ , then the sampled concentration follows the Poisson distribution. In Bayesian inference, the conjugate prior for the rate parameter of the Poisson distribution is the gamma distribution (Fink, 1997). This means that given a same sample of  $N$  measured particles of size  $d$ , and assuming a prior of  $\text{Gamma}(k, \theta)$  the posterior distribution is  $C \sim \text{Gamma}(k + N, \theta)$ . (In Bayesian statistics, the prior is an assumption that quantifies prior knowledge about a quantity before evidence is taken into account, and the posterior distribution quantifies that same quantity after taking evidence into account.) In our case we have little information with which to form a prior, so the best prior is the maximum entropy (i.e. least informative) Jeffreys prior –  $\text{Gamma}(1/2, 0)$  (Lunn et al., 2012). Altogether this means that if we measure  $N$  particles in a volume  $V$ , we get a posterior distribution for the concentration  $C$  of  $C \sim \text{Gamma}(N + \frac{1}{2}, 1/V)$ . This distribution has a mean of  $\frac{N}{V}$ , matching our intuition, and a standard deviation of  $\sqrt{N}/V$ . Sample volume and sampling uncertainty are thus inversely related, and for the same sample volume, the relative uncertainty is larger for lower measured concentrations.

We can also use this distribution to estimate how sample uncertainty propagates into estimated fluxes or parameters of a truncated power law using its posterior predictive distribution — the distribution of possible unobserved values conditional on the observed values — which in this case is the negative binomial (NB) distribution (Gelman et al., 2014). If we measure  $N$  particles in a volume  $V$ , then the distribution of possible unobserved values that accounts for uncertainty in the true concentration given these measured values is  $\text{NB}(N+1/2, 1/(V+1))$ .

To estimate uncertainty in the fitted  $\alpha$  and  $\lambda$  values from  $N(d) = C * d^{-\alpha} * e^{\frac{-d/d_0}{\lambda/\lambda_0}}$  (where  $\lambda_0=1\text{mm}$  and  $d_0 = 1 \text{ mm}$ ), and in the modeled carbon fluxes, we thus draw 100 random samples from  $\text{NB}(N+1/2, 1/(V+1))$  for each particle size class at each sampled place and time. These calculations were run at all places for depths 50 and 300m to retrieve  $\alpha$  and  $\lambda$  and the coefficient

161 of variation of each. We also calculate carbon flux (described in section 2.4) for each of the 100  
 162 simulated PSDs. The coefficient of variation is reported as the standard deviation ( $\sigma$ ) normalized  
 163 by the mean, and relative error ( $error_{rel}$ ) is given by the  $\sigma$  divided by the  $N(d)$ , x 100%.



164  
 165 Figure 2. Theoretical probability of particle concentration ( $N/V$ ) based on observed particle  
 166 number ( $N$ ) or sampling volume ( $V$ ).  
 167

168 The uncertainty associated with sampling volume is visualized using probability densities for  
 169 particle concentrations for either fixed or variable sampling volumes (Figure 2). When sampling  
 170 volume is fixed (and assumed to be 5L), the width of the probability distribution increases  
 171 substantially as particle count increases for an arbitrary size class (compare maroon line to black  
 172 line, Figure 2, left plot). Essentially, if the observed particle count is 5, the true concentration in  
 173 the water column is likely to be between 0.5 and 2 (green line). For fixed concentrations  
 174 (assumed to be 5 particles per L, Figure 2, right plot) and variable sample volumes, the  
 175 probability that the true concentration of particles is accurately measured by the UVP scales with  
 176 sampling volume. Higher sampling volumes (8L, maroon line, Figure 2, right plot) result in  
 177 narrow probability distributions that give higher fidelity to the observed particle concentration.  
 178 Lower sampling volumes (black line, 1L, Figure 2, right plot) have a wider probability

distribution, where it is evident that the true particle concentration can be a factor of 2 (and greater) different than what was observed.

### 2.3 Modeling the observed PSD

Here we modeled observed PSD from the UVP (Figure 1) using a truncated power law, *i.e.* a power law with an exponential cutoff, which is simply a power law multiplied by an exponential function, or

$$N(d) = C * d^{-\alpha} * e^{\frac{-d}{\lambda}}. \quad [1]$$

$N(d)$  is the number of particles within a given size bin and normalized by the bin width,  $d$  is the equivalent spherical diameter, and  $\alpha$  and  $\lambda$  are free parameters. It is implied that both  $d$  and  $\lambda$  are normalized by  $d_0 = \lambda_0 = 1\text{mm}$ , everywhere  $d$  and  $\lambda$  are operated on in this text. The leading constant  $C$  is the concentration at  $d=1\text{ mm}$  divided by  $e^{\frac{1}{\lambda}}$ . The available sizes for  $d$  range from  $1.0 \times 10^{-3}$  to  $26\text{mm}$ , but operationally, the minimum observed particle size from the UVP5 falls into the 128-161 microns size class. Conceptually,  $\alpha$  is a typical power law scaling exponent and  $\lambda$  is the upper limit until which the particle size distribution is well-described by a power law. High values of  $\alpha$  are associated with a steep PSD slope, or a particle assemblage dominated by many small particles relative to larger ones. Low values of  $\lambda$  are associated with a steep decline in  $N(d)$  earlier in the size spectrum (Figure 1b, solid red line compared to red dashed line).

Prior to model fitting, UVP observations of particle concentration ( $\# \text{ L}^{-1}$ ) were multiplied by the sampling volume ( $L$ ) specific to each depth, log10-transformed, and normalized by the bin width (mm) of each size class. We performed a weighted nonlinear optimization of the truncated power law parameters by minimizing the following cost function,

$$\text{cost} = - \sum_{i=1}^n W_i * [\log_{10}(N(d)) - \log_{10}(PSD_{obs})] \quad [2]$$

where  $W_i$  is the weight for each bin ( $i$ ) is the sampling volume divided by the relative sampling error of each size bin, or

$$W_i = \frac{V}{\text{error}_{rel}} \quad [3]$$

The model fitting was performed over the observed particle size interval for each specific instance depending on the depth and location of observations. We constrained  $\alpha$  to be between 0 and 6. The  $\alpha$  range extends slightly beyond the range of observed power law scaling exponents for PSDs (Diehl and Haardt, 1980, Buonassissi and Dierssen 2010), in order to reduce boundary effects during fitting, and we constrained  $\lambda$  to be contained within the bounds of the smallest and largest observed particle size for a particular  $N(d)$ . Because  $\lambda$  spans several orders of magnitude, any reported  $\lambda$  averages for the remainder of this text were calculated using log10 transformed  $\lambda$  values and those averages are then converted into non-log transformed values that are simpler conceptually. We performed this model fit for all 7808 independent locations at the mean of depth bins, or 7.5, 22.5, 47.5, 97.5, 147.5, 222.5, 297.5, 497.5, and 997.5db (hereafter expressed as 10, 25, 50, 100, 150, 225, 300, 500, and 1000m).

The truncated power law model is a better fit to the data than a power law, with an improved adjusted R-squared (accounting for free parameter differences, 0.96 for a truncated power law versus 0.95 for a power law), relative percent error (24% for a truncated power law versus 27% for a power law), and relative bias (i.e.,  $(N(d) - PSD_{obs})/PSD_{obs}$ , 7% for a truncated power law versus 9% for a power law) across all depths. In this study we choose a truncated power law because of the higher overall performance, and because the truncated power law parameters offer more insights about the observed PSD shape than a power law alone.

## 2.4 Carbon flux calculations

The applications of measured in situ PSDs introduce additional uncertainty and error into the derived measurements of interest, including quantifications of carbon flux (Guidi et al., 2008; 2016) and aggregate formation (Guidi et al., 2009). PSDs are ingested within a power law approximation to calculate carbon flux via

$$F = \int_{d_{min}}^{d_{max}} N(d) * A d^b dd, \quad [4]$$

where  $F$  is carbon flux ( $\text{mg m}^{-2} \text{d}^{-1}$ ),  $N(d)$  is the concentration of particles ( $\# \text{L}^{-1}$ ) with a mean equivalent spherical diameter ( $d$ , mm), and  $A$  (12.5) and  $b$  (3.81) are free parameters that were first optimized in Guidi et al. (2008) using all available UVP versions with a shared size interval

of 250 microns to 1.5mm, and with sampling volumes ranging from 0.28 to 10.5L. The function is integrated over the range of size classes available. While  $A$  and  $b$  are empirically derived, they conceptually arise from a general mechanistic model that incorporates sinking velocity (via Stokes' law, a power law) and carbon content of a particle (modeled as a power law). The product of sinking velocity ( $w(d) = \beta d^2$ ) and carbon content ( $m(d) = \alpha d^3$ , both power laws) are modeled as a power law, providing the  $Ad^b$  term in equation 4. We note that the power law formulation for carbon content assumes that all particles of a given size have the same carbon content and sinking speed, which is a flawed assumption given current understanding of particle characteristics. Given typical power law fits for  $N(d)$ , equation 4 implies an infinite flux with increasing particle size, as well as a consistent size-to-flux relationship for equally sized cells, which will be violated for cells of different density and/or lability. We argue here that any PSD-derived flux formula must be aligned with the known uncertainties of the PSD observations. Particularly, the value of  $d_{\max}$  is important if a power law  $N(d)$  is selected because the counts of  $N(d_{\max})$  become negligible due to sampling. The value of  $d_{\max}$  is also important when comparing across different UVP versions with different size ranges.

We calculated flux using direct observations of UVP PSD via equation 4, as well as using the modeled PSD derived from equation 1, or

$$F_m = \sum C * d^{-\alpha} * e^{\frac{-d}{\lambda}} * Ad^b. \quad [5]$$

Where  $F_m$  denotes flux from the modeled number distribution. We tested different values of  $A$  and  $b$  to reflect the different values used (Kiko et al., 2017, Kriest, 2002, Alldredge, 1998), where  $A = 2.8$  and  $b = 2.24$ , noting that the latter  $b$  value might be a more realistic size-sinking scaling exponent than  $b = 3.81$  (Cael et al., 2021), because the value of  $b$  in the Guidi et al., (2008) work is not the size-sinking speed relationship, but rather the optimized value when compared to observations over a defined size range. We note that we are less interested in the specific values of  $A$  and  $b$ , but rather how the fundamental characteristics of flux's functional form affect its outcome given modeled sampling uncertainties, as in Cael and Bisson, (2018). For the remainder of this paper we use  $A = 2.8$  and  $b = 2.24$  because those values are meant to

represent flux more realistically across the range of sizes and particles thought to contribute to flux.

One advantage of the modeled PSD in this study is that it can be used to extract the particle number outside the range of observed particle sizes. To quantify the sensitivity of the flux relationship to different sizes, we included bins two sizes smaller than the first size bin observed, as well as two bins larger than the last size bin observed, for each PSD model. Operationally this meant including 80 microns to anywhere from 1 mm to 26 mm for the size interval. The objective was not to extrapolate widely beyond what has been observed, but rather to include size classes within neighboring bins relative to what was actually seen by the UVP, in order to assess the sensitivity of flux derived from the UVP. Carbon flux calculated using a wider interval for particle sizes was compared to flux calculated from the observed PSD size range. In this study we are not concerned about the performance of the flux model (as has been done in other studies, Guidi et al 2008, Fender et al., 2019). We instead ask, ‘how does using a more complete PSD affect flux calculations?’

## 4 Results and Discussion

### 4.1 Global $\alpha$ and $\lambda$ values

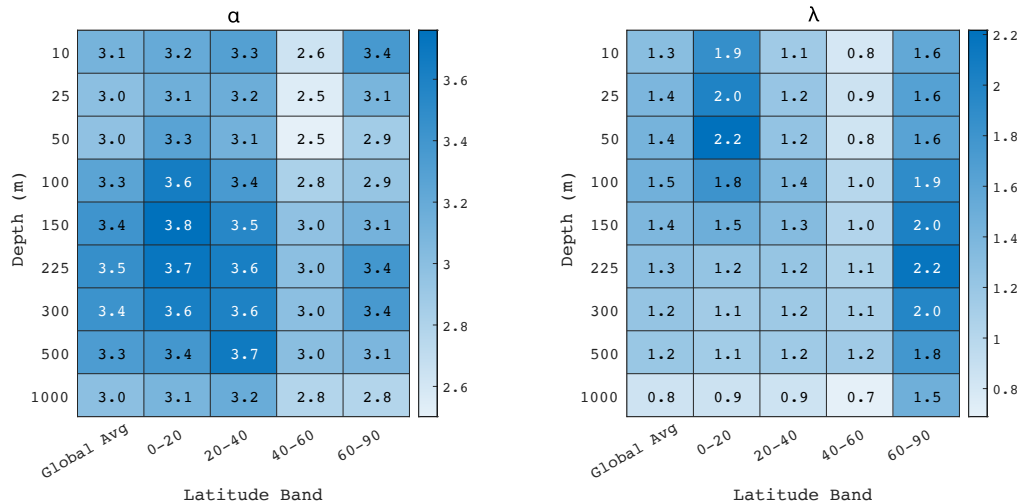
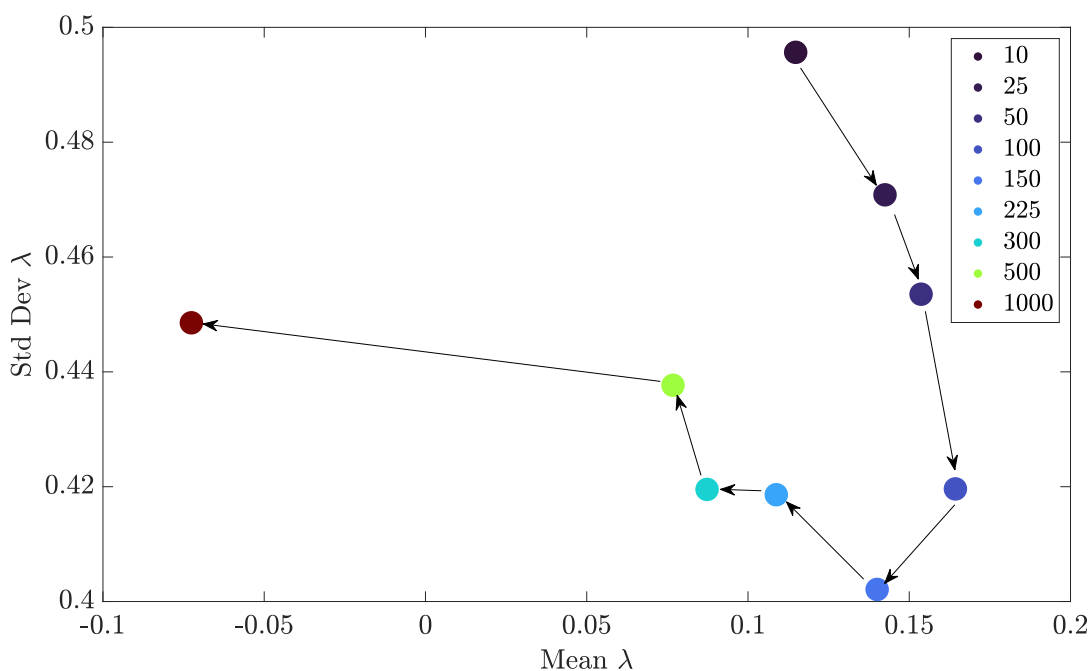


Figure 3. Heatmap of  $\alpha$  (left) and  $\lambda$  (right, normalized to  $\lambda_0 = 1$  mm) based on latitudinal bands and depth.

Global values of retrieved  $\alpha$  and  $\lambda$  reveal patterns across space and depth (Figure 3, Supplementary Figures 1,2). The highest average  $\alpha$  values (3.8) are in moderate depths (100-300



288 m) for places equatorward of 20 degrees. In general,  $\alpha$  varies throughout the water column, with  
 289 larger values between depths of 150 and 500m, and lower values at the surface and at 1000m  
 290 depth.  $\lambda$  generally decreases with depth, where the global average  $\lambda$  decreases from 1.3 at 10m to  
 291 0.8 at 1000m, and in all places the surface  $\lambda$  value exceeds  $\lambda$  at 1000m, if only slightly.



292  
 293 Figure 4. Standard deviation in  $\log_{10}(\lambda)$  plotted against the mean  $\log_{10}$ -transformed  $\lambda/\lambda_0$   
 294 (where  $\lambda_0 = 1\text{mm}$ ) based on depth (colors). Arrows denote the transition from shallow (top right)  
 295 to deep (top left) samples.

296 The standard deviation of  $\lambda$  is highest for the surface ocean and deepest observations at  
 297 1000m (Figure 4). In between the surface and depth,  $\lambda$  standard deviation and  $\lambda$  mean (all  $\log_{10}$   
 298 transformed) have a qualitative clockwise trend (Figure 4) where the average  $\lambda$  changes only  
 299 subtly at depths  $< 1000\text{m}$  while the standard deviation decreases from  $\sim 10^{0.5}$  to  $\sim 10^{0.4}$ . The  
 300 variability (given by the standard deviation) in  $\lambda$  decreases with depth up to 150m but thereafter  
 301 increases to a smaller degree. These results do not necessarily mean there are no big particles (or  
 302 ‘dragon kings’, Bochdansky et al., 2016) in the deep, but rather the UVP5 is not observing them.

303 The model parameters  $\alpha$  and  $\lambda$  from the truncated power law fit to observed PSD reflect  
 304 the relative dominance of small versus large particles, and also indicate the heavy (or not) tail-  
 305 ness of the size distribution. In essence,  $\alpha$  mostly quantifies the mid-range behavior in the PSD  
 306 and  $\lambda$  mostly quantifies the upper-range behavior. Although the model is statistical in nature,

quantifying the PSD slope and size interval where a power law is applicable gives more information about the shape of the PSD than slope alone. In other words, conventional power law fits to PSD assume that a power law is appropriate over the entire size distribution, and the parameter power law model may not be ideal for characterizing the PSD shape from the UVP.

Lower values of  $\alpha$  indicate a higher contribution of large particles relative to small ones, and lower  $\lambda$  values indicate that the power law breaks down at smaller particle sizes (and therefore we expect very few larger particles in the PSD compared to higher  $\lambda$ ). It follows, then, that places with shifts in  $\alpha$  or  $\lambda$  indicate shifts in the shape of the PSD that may be biogeochemically important. Without coincident observations of particle composition, it is not sensible to say whether or not changes in the PSD shape may specifically be due to e.g., aggregation/disaggregation, ingestion/egestion and vertical transport of zooplankton, bacterial remineralization processes, and so on. However, the clear decrease in global average  $\lambda$  with depth implies that there are fewer large particles at deeper depths in the ocean on average (as observed by the UVP). We note that the particle module on Ecotaxa does not discriminate living from non-living particles, so it is possible that changes in  $\lambda$  will scale with changes in zooplankton abundance and size.

Trends in  $\alpha$  are less straightforward. In nearly every latitudinal band,  $\alpha$  increases at moderate depths, indicating a higher prevalence of small particles, then decreases at deeper depths. The reported  $\alpha$  and  $\lambda$  values here may be useful in future studies to guide improvements to the PSD-derived flux relationship. More work is needed to investigate how the shapes of the PSD (including statistics for the observed PSD's tail as described here) influence carbon flux. For example, can variations in  $\lambda$  values across depth/season/place be used to predict aggregation/disaggregation, or the sinking of fecal pellets? How might variations in  $\alpha$  and/or  $\lambda$  along isopycnals (or depth, to first order) inform improved parameterizations for the PSD-derived carbon flux model?

## 4.2. Extrapolation and sampling uncertainties

We acknowledge that it is not sensible to calculate flux in the surface ocean using PSD observations that are unlikely to comprise sinking particles, when considering either the UVP or another PSD-resolving instrument. Here we consider particles  $2\mu\text{m}$  and above, and we use the following scaling argument to estimate that any sinking by particles  $<2\mu\text{m}$  can be considered

negligible. For a particle to be considered as sinking, its vertical transport from sinking must be greater than its vertical transport from ambient turbulent fluid motions. Balancing the two processes, a particle's minimum sinking speed  $w_{min} \sim \sqrt{\kappa/\tau}$  will be  $\sim 3 \text{ m day}^{-1}$ , assuming  $\kappa \sim 10^{-4} \text{ m}^2 \text{ s}^{-1}$  [Munk, 1966] and  $\tau = 1 \text{ day}$  is a characteristic measurement, diel, and small particle lifetime timescale. Then if particles' sinking speeds scale approximately as  $w(d) \sim 100 d^{-0.63} \text{ m day}^{-1}$  (Kriest et al 2002, Cael et al, 2021),  $w \sim w_{min}$  when  $d \sim 2 \mu\text{m}$ . Note also  $2 \mu\text{m}$  is roughly the smallest particle size that can be estimated by other instruments in a sinking or flux context (Cael and White, 2020).

There are particles that contribute to flux that are not captured by the UVP's sampling volume and specifications. Under what conditions or assumptions are the observed particles sufficiently representative of the total particle population's flux? Figure 5 shows how particles outside the UVP5-observed size range contribute to total flux, for a truncated power-law particle size distribution and a power-law size-flux relationship. If  $b$  is the exponent dictating how sinking and mass (or carbon or other elemental content) together scale with particle size, and  $\alpha$  is the exponent dictating how abundance scales with particle size within the power-law scaling range, the contribution to flux by particles of a given size will be determined by their difference,  $b - \alpha$ . The contribution of large particles will also be determined by  $\lambda$ , the particle size where the power law is truncated.

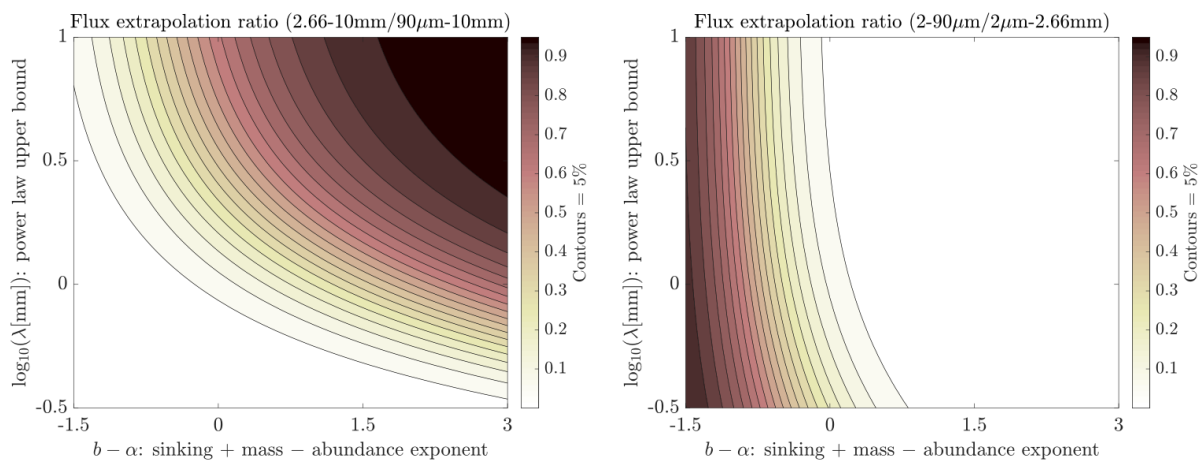


Figure 5. Theoretical flux extrapolation ratio as a function of the difference between  $b$  (sinking + mass, = 3.81 or 2.24) and  $\alpha$ , and the upper bound particle size where a power law is appropriate.

Figure 5a shows the fraction of flux in the 90 $\mu$ m-10mm particle ESD range for which 2.66-10mm particles are responsible, as a function of  $b - \alpha$  and  $\lambda$ . We note that this is a conceptual figure that serves only to illustrate under what conditions particle fluxes can be dominated by particles of different sizes. Clearly both parameters play a role; when  $\lambda$  and  $b - \alpha$  are both small, meaning large particles are rare and particles' sinking-and-mass size-dependence is weaker than particles size-abundance relationship, large particles contribute very little to total flux so almost none of the flux occurs in the 2.66-10mm size range. When either  $\lambda$  or  $b - \alpha$  are large, however, particles in this range do contribute appreciably to overall flux. When both  $\lambda$  and  $b - \alpha$  are large, meaning the power-law distribution extends out to multi-millimeter particles and the sinking-and-mass size dependence of particles is strong relative to particles' size-abundance relationship, most of the flux actually can occur in this 2.66-10mm size range. In contrast, Figure 5b shows the same but for small particles, comparing 2-90 $\mu$ m particles against 2 $\mu$ m-2.66mm particles. In this case the dependence on  $\lambda$  is unsurprisingly very weak, but we do see that as long as approximately  $b - \alpha < 0$ , *i.e.* that particle abundance scales more strongly with size than particles' sinking and mass, much or even most of the flux occurs in particles <90 $\mu$ m. Although the UVP does not measure particles smaller than 90  $\mu$ m, these figures underscore that accurate UVP-based flux estimates require understanding the controls on and variability of particles' sinking-size and mass-size relationships, the prevalence of large particles, and the slope of the particle size distribution. We include them to demonstrate that sampling uncertainty includes uncertainty due to particles outside the detection limit of the UVP or any PSD-resolving instrument.

There is high variability in retrieved  $\alpha$ ,  $\lambda$ , and carbon flux arising from the sample volume uncertainty using the observed size range from UVP observations, as calculated from 100 simulations with varying  $N(d)$  (informed by the observed  $N(d)$  and sampling volume) for all locations in this study at 50 and 300m (Figure 6, Supplementary Figure 3, see also section 2.2 for procedure). Across all three variates, the coefficient of variation is smallest for  $\alpha$  at either depth than it is for  $\lambda$  and carbon flux. The median coefficient of variation for  $\alpha$  is ~25% at both depths, while the median coefficient of variation for  $\lambda$  is nearly 60% for the 50m case, and 55% for the 300m case. The coefficient of variation for carbon flux arising from the sampling volume uncertainty is highest for deep particles (~65-70%) compared to the 50m case (50-55%). The width of the coefficient of variation distributions varies for all three variates as well, with  $\alpha$

showing the tightest range, followed by  $\lambda$  and carbon flux. We emphasize that the coefficient of variations reported here are due only to measurement error and not due to natural variability, which we could not fully characterize due to lack of repeat data (see Supplementary Figure 4). As a test of how larger sampling volumes may influence the coefficient of variation in  $\alpha$ ,  $\lambda$ , and carbon flux, we also ran the bootstrapping procedure using simulated sampling volumes that are double the observed sampling volume. Doubling the sample volume reduces the coefficient of variation in carbon flux to a median of 56% compared to a median of 67% in the 300m case (Supplementary Figure 5). Note that we did not adjust the  $N(d)$  (doing so would preserve the particle concentration) so that we could isolate the relative effect of enhancing sampling volume in a statistical sense.

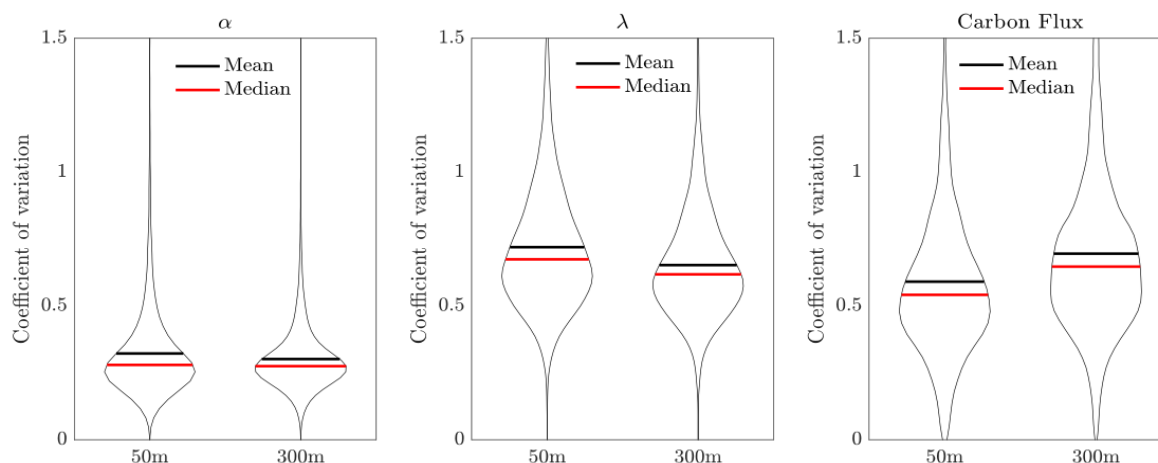
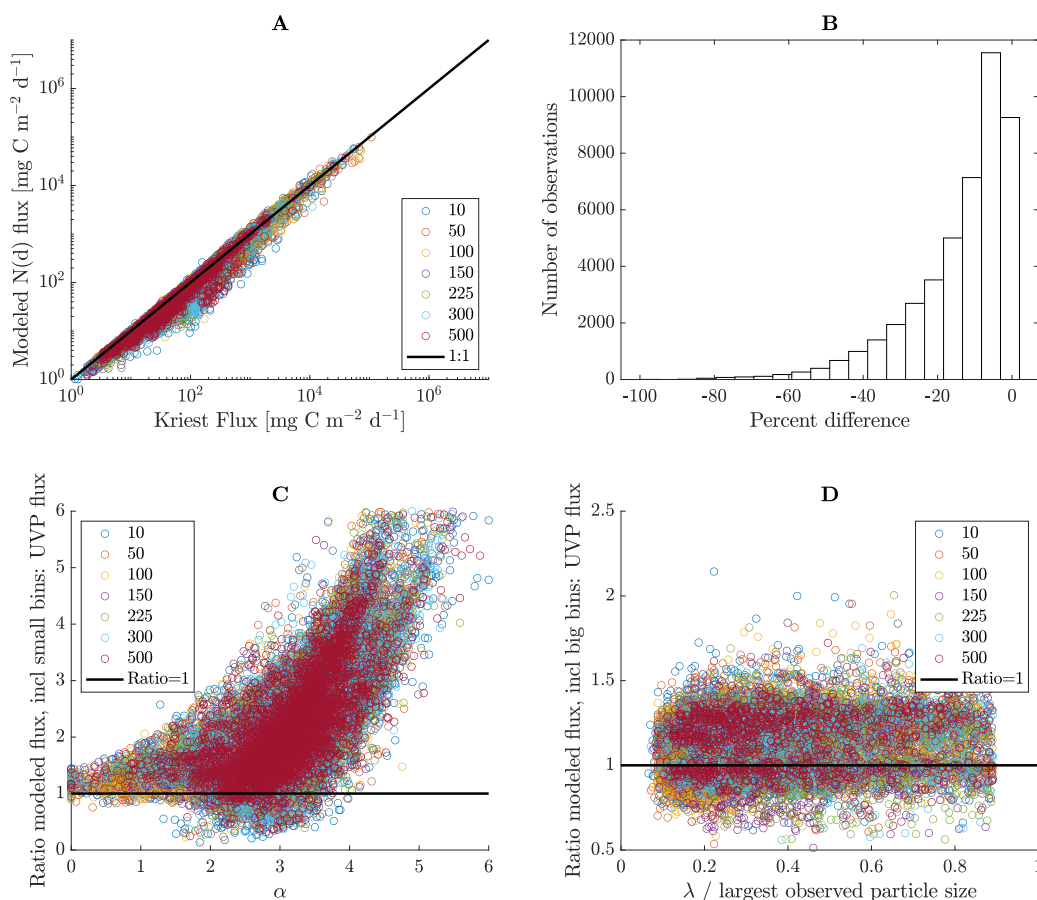


Figure 6. Violin plots for coefficient of variation in  $\alpha$  (left),  $\lambda$  (middle) and carbon flux based on either 50 m or 300m (resulting from the bootstrap procedure). The coefficient of variation reported in this figure is due only to the sampling volume uncertainty.

### 4.3 Sensitivity of modeled carbon flux to particle size

Carbon flux calculations using observed and modeled PSD (over a shared size range, i.e., the fixed lower limit of 128  $\mu\text{m}$  for each profile and an upper limit dictated by the largest observed particle size) are well correlated as expected, agreeing within 10% for the majority of locations and depths (Figure 7A and Figure 7B). The flux relationship is highly sensitive to the inclusion of smaller particle sizes. In some cases, the ratio of flux calculated using two size bins smaller than observed to the ratio of flux calculated using only observed particle sizes is nearly 6. The high degree of sensitivity to small particles directly scales with the  $\alpha$  value of the modeled

415 PSD. For small  $\alpha$  (indicating a dominance of larger particles relative to small), the inclusion of  
 416 smaller size classes makes relatively little difference in the flux calculations (Figure 7C).  
 417 However, for  $\alpha$  larger than 2, the sensitivity of flux to smaller size classes is substantial, with  
 418 relative differences exceeding a factor of 2.



419  
 420 Figure 7. A. Flux comparisons between modeled N(d) flux (y axis) and N(d) flux from UVP  
 421 observations ('Kriest flux') over the same particle size range. B. Histogram of percent difference  
 422 (relative to 'Kriest flux') between all flux determinations in A. C. The ratio of modeled N(d) flux  
 423 (including 2 size bins smaller than the observed size range) to observed N(d) flux as a function  
 424 of depth (colored dots) and alpha value. Black line represents equivalent fluxes. D. The ratio of  
 425 modeled N(d) flux (including 2 size bins larger than the observed size range) to observed N(d)  
 426 flux as a function of depth (colored dots) and lambda value relative to largest observed particle  
 427 size. Black line represents equivalent fluxes.

428 On the flip side, the flux relationship with PSD is much less sensitive to the inclusion of  
 429 larger size bins relative to what was observed (Figure 7D). Recall that the modeled PSD in this

scenario contains two size bins larger than what was observed. It is common for only a single particle (or none at all) to be observed at the largest observable size class, so modeled concentrations are accordingly low at the high end of the particle size spectrum. The few large particles in bigger bin sizes stands in contrast to smaller sized particles, which become more numerous as size decreases. We choose to compare the two flux scenarios across the ratio of  $\lambda$  relative to the largest observed particle size (the x-axis in Figure 7D). When this ratio is small, the modeled PSD breaks down from a power law into an exponential decay function at lower size classes. When this ratio is 1, the entire PSD can be modeled using a power law. The relative difference of flux calculated using modeled PSD for larger size classes, to flux calculated using the observed PSD, is around 50% and there is no obvious relationship with the  $\lambda$  value. Although a change of flux by 50% is non-trivial, it is modest compared to changes in flux exceeding 5-fold, as is the case when including smaller particle sizes.

The sensitivity of PSD-derived flux to either small or large particles is robust to changes in the free parameter values of **A** and **b**. When the Guidi et al., 2008 formulation was applied (Supplementary Figure 6), a similar sensitivity was observed, although the overall magnitude of flux was much enhanced compared to the Kriest et al., (2002) formulation. Ideally, any biogeochemical model will not be sensitive to the inclusion of either small ( $< 128 \mu\text{m}$ ) or large size classes ( $> 1\text{mm}$ ) because small particles are not thought to contribute the bulk of carbon flux (see Michaels and Silver, 1988; Bopp et al., 2005), and because large particles are rarely observed and highly uncertain (and so any model relying on large particles for flux would be highly uncertain as well). In this study we found that no matter which flux parameter values are used (i.e., the empirically derived Guidi et al., 2008 values or the more mechanistic Kriest et al., 2002 values) the power law flux relationship is still highly sensitive to the inclusion of small particles. This sensitivity is a surprising result, and likely arises because the high abundance of small particles overcomes their relatively small diameter (in this case, 80 microns) to contribute a large amount of flux (up to 6 times the amount of carbon flux calculated using a minimum particle size of 128 microns). If we included even smaller size classes we expect the flux to increase further. The idea that small particles can contribute substantial flux stands contrary to what is expected from observations of sinking particles in a natural setting (Cael et al., 2021 and refs therein). However, some flux models also predict a larger contribution of small sinking flux (e.g., Bisson et al., 2020, Siegel et al., 2014) than is expected (Durkin et al., 2015, Cael and

White, 2020, Cael et al., 2021). We note that the small particles are not thought to contribute substantially to flux when it is assumed that these small particles are formed in the surface, because they will be remineralized in their 100s of meters transit to depth. However, small particles may actually dominate flux in deeper waters through disaggregation processes (Kiko et al., 2017, Bianchi et al., 2018).

In this study, we found that the flux relationship is moderately sensitive to the inclusion of larger particles. One reason for this is because the inclusion of larger bin sizes did not introduce many more particles within this size range, since modeled  $N(d)$  is often low (if not zero) for large particles. In the real ocean, rare large ( $> 1$  mm) particles can contribute a substantial amount of flux (Bochdanský et al., 2016), but these particles may be missed by the UVP due to sampling volume limitations. We recommend accounting for uncertainty in larger particles based on the sampling volume.

#### 4.4 Limitations of using the UVP to assess particle flux

The primary uncertainties associated with carbon flux derived from UVP observations are 1) assuming the parameters  $A$  and  $b$  in equation 4 are globally valid at all depths, for all UVP models, and across all size classes 2) the UVP's pixel-to-size uncertainty, 3) error associated with particle detection due to image contrast and porous aggregates (that may appear as many small particles separated by holes) 4) the sampling uncertainty of the PSD, 5) the size to sinking rate uncertainty, and 6) the size to carbon mass uncertainty. We note that the error associated with #3 is likely to be the smallest of all errors presented because the UVP is built to detect near transparent particles in water. In this study we focused on quantifying the sampling uncertainty of the PSD (#4 as described above), as well as how this uncertainty propagates into a commonly used carbon flux model. Ultimately, the sensitivity of the flux relationship to smaller particles was a surprising result of this study, and it invites a re-examination to the flux model in order to guide future work.

While some attention has been paid to optimizing the parameters ( $A$ ,  $b$ ) of the carbon flux model (Guidi et al., 2008, Fender et al., 2019), it seems a larger problem is in the foundation of the flux model itself. We calculated carbon fluxes incorporating the reported Guidi et al., 2008 parameter standard deviations to learn how carbon flux is uncertain based on parameter value uncertainty. Uncertainty in  $A$  resulted in a median 21% relative error in carbon flux while



uncertainty in ***b*** resulted in median 19% relative error using the profiles in this study at all depths. Using the Guidi parameters instead of the Kriest parameters results in median differences approaching a factor of 2 (compared to factors of 6 when incorporating 80-128 $\mu$ m particles).

Given the large uncertainty also associated with sampling volume, we recommend optimizing the flux model using the same UVP version, or by accounting for uncertainty directly in the model optimizations (e.g., Bisson et al., 2018). We note that the Guidi et al., 2008 study used a size interval of 250 microns to 1.5mm in order to incorporate older UVP versions (with sampling volumes ranging from 0.28 – 10.5L) and did not use UVP-5 data. However, although the Guidi et al., 2008 parameters were optimized over a different size interval than was used here, the specific values of ***A*** and ***b*** will not modify the sensitivity of flux to small size classes (compare Figure 7 with Supplementary Figure 6). Normally, ***A*** and ***b*** values are optimized within the boundaries of the size spectrum imaged by the UVP, and therefore any regionally optimized PSD-flux relationship is not necessarily problematic to use, even though the theoretical underpinnings of such a relationship are imperfect.

It can be instructive to think of the flux model as a transfer function (***A**d*<sup>*b*</sup>**) that is multiplied by ***N*(*d*)**. The transfer function is a monotonic power law that grows substantially at larger particle sizes. Therefore, if anything, the flux model is expected to be sensitive to rare instances of large particles, depending on ***b*** versus  $\alpha$ . If particles in the ocean grew indefinitely, infinite flux would be expected from this relationship. On the other hand, infinite flux is possible with smaller particle sizes if the concentration of particles grows more than particle size decreases, as was the case in this study. If the true PSD were not monotonic (i.e., increasingly higher concentrations of particles at lower particle sizes), a monotonic flux model (such as the power law used here) may be sufficient. What instead might be needed is a transfer function that quantifies the probability of a given particle size to sink. Small sized particles would accordingly have low probability, as would larger particles that are ultimately living zooplankton (or fish in the extreme case). Medium to medium-large sized particles would have moderate to high probability of becoming carbon flux, which might yield a more realistic carbon flux model. More work is needed to improve the PSD-derived carbon flux relationship, and especially the size to sinking carbon uncertainty, which is outside the scope of this paper.

Finally, particles sized by the UVP include living and non-living particles, which adds uncertainty to flux calculations derived from PSD alone. If only non-living particles were

assembled for use by modelers and the rest of the community, the uncertainty associated with ambiguity of large particles (*i.e.*, is it a zooplankter or aggregate?) would be reduced. Indeed, one study (Kiko et al., 2020) found reduced variability in PSD-derived carbon flux, during which living objects and artefacts with an equivalent spherical diameter larger than 1mm were removed from the UVP5 image dataset so that only detrital particles were used to calculate flux in this size range.

#### 4.5 Future applications of using a truncated power law to model PSD

In this study we found enhanced performance of the modeled PSD when using a truncated power law rather than a power law. Truncated power laws offer more information about a PSD distribution compared to a power law because the behavior of the distribution is characterized through two main parameters ( $\alpha$ ,  $\lambda$ ) rather than just one ( $\alpha$ , in the case of a power law). There are several applications to using a truncated power law besides what has been explored here. First, with an improved model for PSD, one could extrapolate the PSD to quantify the carbon content of particles in the particulate fraction globally. Second, extrapolating the PSD using a truncated power law may enable improved respiration rates as derived from UVP observations, as current estimates are limited by the size resolved by the UVP (Kavelage et al., 2015, Thomsen et al., 2019). Third, the current UVP data hosted by Ecotaxa includes both living and non-living particles. Future work may explore whether or not the  $\lambda$  values will be useful to identify when the PSD spectrum transitions from particles to larger zooplankton (Forest et al., 2012).

#### 5 Recommendations for future work

Although we chose to focus on sampling uncertainties and how they influence carbon flux values, there are outstanding issues with the assumed size to sinking rate uncertainty, and size to carbon mass uncertainty. These uncertainties may be reduced in future work by using existing information from UVP images. Below, we mention a few possible avenues to address uncertainty associated with the UVP carbon flux model.

1. *Sampling uncertainty*: Future UVP designs can reduce sampling uncertainty by increasing the sampling volume of the instrument. Current UVP designs can reduce

sampling uncertainty to some extent by performing multiple casts of repeat sampling. More work needs to be done in order to distinguish aggregates from living plankton for particles in the observable size range, preferentially down to 2  $\mu\text{m}$  size.

2. *Size to sinking uncertainty*: Although unconventional, a UVP fastened to a Lagrangian sediment and/or gel trap that is oriented with a side-viewing camera may allow sinking speed to be assessed via several images, where sediment trap flux, particle sinking speeds from a gel trap, and particle size information would be coupled and coincident. Similarly, in situ sinking speeds could be obtained using Particle Imaging Velocimetry (Cartwright et al. 2013), optimally during the upcast of a CTD/UVP profile. This logistically less demanding approach could yield PSD observations over the entire water column and coincident particle sinking speed observations at different water depths. Targeting blooms of different organisms with UVP observations may also help to improve size-sinking relationships. Direct observations that better constrain the size-sinking scaling relationship globally, in different environments, and/or for different particle types is essential for improving uncertainties in UVP-derived fluxes. (Cael et al., 2021).

3. *Size to carbon content uncertainty*: Dense particles may have a different reflectance than less dense particles (based on the fractal dimension) which might provide a way to semi-quantitatively assess particle composition from the contrast of the images. If such an exercise is possible, the contrast of images may add information content to the flux relationship so particle size and concentration are not the only variables. Further classification of particle images into e.g. fecal pellets, marine snow and other types of detrital matter and the application of class specific size to carbon ratios might also reduce the errors in flux calculation (Durkin et al., 2021). Finally, due to remineralization, carbon content might also decrease over depth without large changes in size or appearance of the particles. Therefore, further work is needed to characterize the carbon to size relationship of detrital particles at different depths.

Although we did not investigate the uncertainty associated with the conversion of UVP pixels to a particle size, more work is needed to characterize any error and uncertainty arising from particle shape differences and assumed spherical diameters. Improved edge detection of pixels is

needed, as well as a sensitivity analysis of how threshold values for edge detection affect particle size (as is also advised by Giering et al., 2020).

## **6 Summary**

In this study we focused on UVP sampling uncertainties and how they propagate into derived estimates of carbon flux. The PSD observations from the UVP5 have a sampling uncertainty  $\sqrt{N}/V$ . The sampling uncertainty of PSD observations results in an uncertainty slightly greater than 50% for carbon flux. The extrapolated carbon flux from the UVP is based on a relationship that is highly sensitive (up to 6-fold different) to the inclusion of particles slightly smaller than what was observed. We advocate for a revised carbon flux relationship that is possibly non-monotonic and considers the probability of a given particle to become carbon flux. In the absence of an improved carbon flux relationship, carbon flux calculations should be made using parameters specific to a particular region and depth to prevent large errors. Future work may benefit by using UVP data in unconventional ways, such as coupling a UVP and sediment trap in the same water mass, and/or by performing image analysis on the particular pixels comprising a particle.

## **Acknowledgments and Data Statement**

Cael was supported by the National Environmental Research Council (NE/R015953/1) and the Horizon 2020 Framework Programme (820989, project COMFORT, our common future ocean in the Earth system—quantifying coupled cycles of carbon, oxygen, and nutrients for determining and achieving safe operating spaces with respect to tipping points). The work reflects only the authors' view; the European Commission and their executive agency are not responsible for any use that may be made of the information the work contains.

RK acknowledges support via a "Make Our Planet Great Again" grant of the French National Research Agency within the "Programme d'Investissements d'Avenir"; reference "ANR-19-MPGA-0012", the BMBF funded project "CUSCO" and funding from the European Union's Horizon 2020 research and innovation programme for the TRIATLAS project under grant agreement No 817578. The UVP data used in this study can be accessed via PANGAEA, <https://doi.pangaea.de/10.1594/PANGAEA.924375>. Log ins are required for downloading, and the data span 2008-2020. More processing details are in Kiko et al., 2021.

## References

- Allredge, A. L., & Gotschalk, C. (1988). In situ settling behavior of marine snow 1. *Limnology and Oceanography*, 33(3), 339-351.
- Allredge, A. (1998). The carbon, nitrogen and mass content of marine snow as a function of aggregate size. *Deep Sea Research Part I: Oceanographic Research Papers*, 45(4-5), 529-541.
- Bianchi, D., Weber, T. S., Kiko, R., & Deutsch, C. (2018). Global niche of marine anaerobic metabolisms expanded by particle microenvironments. *Nature Geoscience*, 11(4), 263-268.
- Bisson, K. M., Siegel, D. A., DeVries, T., Cael, B. B., & Buesseler, K. O. (2018). How data set characteristics influence ocean carbon export models. *Global Biogeochemical Cycles*, 32(9), 1312-1328.
- Bisson, K., Siegel, D. A., & DeVries, T. (2020). Diagnosing mechanisms of ocean carbon export in a satellite-based food web model. *Frontiers in Marine Science*, 7, 505.
- Bochdansky, A. B., Clouse, M. A., & Herndl, G. J. (2016). Dragon kings of the deep sea: marine particles deviate markedly from the common number-size spectrum. *Scientific reports*, 6(1), 1-7.
- Bopp, L., Aumont, O., Cadule, P., Alvain, S., & Gehlen, M. (2005). Response of diatoms distribution to global warming and potential implications: A global model study. *Geophysical Research Letters*, 32(19).
- Boss, E., Twardowski, M. S., & Herring, S. (2001). Shape of the particulate beam attenuation spectrum and its inversion to obtain the shape of the particulate size distribution. *Applied Optics*, 40(27), 4885-4893.
- Buonassissi, C. J., & Dierssen, H. M. (2010). A regional comparison of particle size distributions and the power law approximation in oceanic and estuarine surface waters. *Journal of Geophysical Research: Oceans*, 115(C10).

- Cael, B. B., Cavan, E. L., & Britten, G. L. (2021). Reconciling the size-dependence of marine particle sinking speed. *Geophysical Research Letters*, 48(5), e2020GL091771.
- Cael, B. B., & White, A. E. (2020). Sinking versus suspended particle size distributions in the North Pacific Subtropical Gyre. *Geophysical Research Letters*, 47(15), e2020GL087825.
- Cael, B. B., & Bisson, K. (2018). Particle flux parameterizations: Quantitative and mechanistic similarities and differences. *Frontiers in Marine Science*, 5, 395.
- Cartwright, G. M., Friedrichs, C. T., & Smith, S. J. (2013). A test of the ADV-based Reynolds flux method for in situ estimation of sediment settling velocity in a muddy estuary. *Geo-Marine Letters*, 33(6), 477-484.
- Chase, A. P., Kramer, S. J., Haëntjens, N., Boss, E. S., Karp-Boss, L., Edmondson, M., & Graff, J. R. (2020). Evaluation of diagnostic pigments to estimate phytoplankton size classes. *Limnology and Oceanography: Methods*, 18(10), 570-584.
- Dall'Olmo, G., Westberry, T. K., Behrenfeld, M. J., Boss, E., & Slade, W. H. (2009). Significant contribution of large particles to optical backscattering in the open ocean. *Biogeosciences*, 6(6), 947.
- Diehl, P., & Haardt, H. (1980). Measurement of the spectral attenuation to support biological-research in a plankton tube experiment. *Oceanologica Acta*, 3(1), 89-96.
- Durkin, C. A., Buesseler, K. O., Cetinić, I., Estapa, M. L., Kelly, R. P., & Omand, M. (2021). A visual tour of carbon export by sinking particles. *bioRxiv*.
- Fender, C. K., Kelly, T. B., Guidi, L., Ohman, M. D., Smith, M. C., & Stukel, M. R. (2019). Investigating particle size-flux relationships and the biological pump across a range of plankton ecosystem states from coastal to oligotrophic. *Frontiers in Marine Science*, 6, 603.

- Fink, D. (1997). A compendium of conjugate priors. See [http://www. people. cornell. edu/pages/df36/CONJINTRnew% 20TEX. pdf](http://www.people.cornell.edu/pages/df36/CONJINTRnew%20TEX.pdf), 46.
- Forest, A., Stemmann, L., Picheral, M., Burdorf, L., Robert, D., Fortier, L., & Babin, M. (2012). Size distribution of particles and zooplankton across the shelf-basin system in southeast Beaufort Sea: combined results from an Underwater Vision Profiler and vertical net tows. *Biogeosciences*, 9(4), 1301-1320.
- Gelman, A., Carlin, J. B., Stern, H. S., Dunson, D. B., Vehtari, A., & Rubin, D. B. (2014). Bayesian Data Analysis, volume third ed.
- Giering, S. L., Cavan, E. L., Basedow, S. L., Briggs, N., Burd, A. B., Darroch, L. J., ... & Lindsay, D. J. (2020). Sinking organic particles in the ocean—flux estimates from in situ optical devices.
- Guidi, L., Jackson, G. A., Stemmann, L., Miquel, J. C., Picheral, M., & Gorsky, G. (2008). Relationship between particle size distribution and flux in the mesopelagic zone. *Deep Sea Research Part I: Oceanographic Research Papers*, 55(10), 1364-1374.
- Guidi, L., Stemmann, L., Jackson, G. A., Ibanez, F., Claustre, H., Legendre, L., ... & Gorsky, G. (2009). Effects of phytoplankton community on production, size, and export of large aggregates: A world-ocean analysis. *Limnology and Oceanography*, 54(6), 1951-1963.
- Guidi, L., Chaffron, S., Bittner, L., Eveillard, D., Larhlimi, A., Roux, S., ... & Coelho, L. P. (2016). Plankton networks driving carbon export in the oligotrophic ocean. *Nature*, 532(7600), 465-470.
- Gorsky, G., Picheral, M., & Stemmann, L. (2000). Use of the Underwater Video Profiler for the study of aggregate dynamics in the North Mediterranean. *Estuarine, Coastal and Shelf Science*, 50(1), 121-128.

Haight, Frank A. *Handbook of the Poisson distribution*. No. 519.23 H3. 1967.

Jonasz, M., & Fournier, G. (2011). *Light scattering by particles in water: theoretical and experimental foundations*. Elsevier.

Karp-Boss, L., Azevedo, L., & Boss, E. (2007). LISST-100 measurements of phytoplankton size distribution: Evaluation of the effects of cell shape. *Limnology and Oceanography: Methods*, 5(11), 396-406.

Kalvelage, T., Lavik, G., Jensen, M. M., Revsbech, N. P., Löscher, C., Schunck, H., ... & Kuypers, M. M. (2015). Aerobic microbial respiration in oceanic oxygen minimum zones. *PloS one*, 10(7), e0133526.

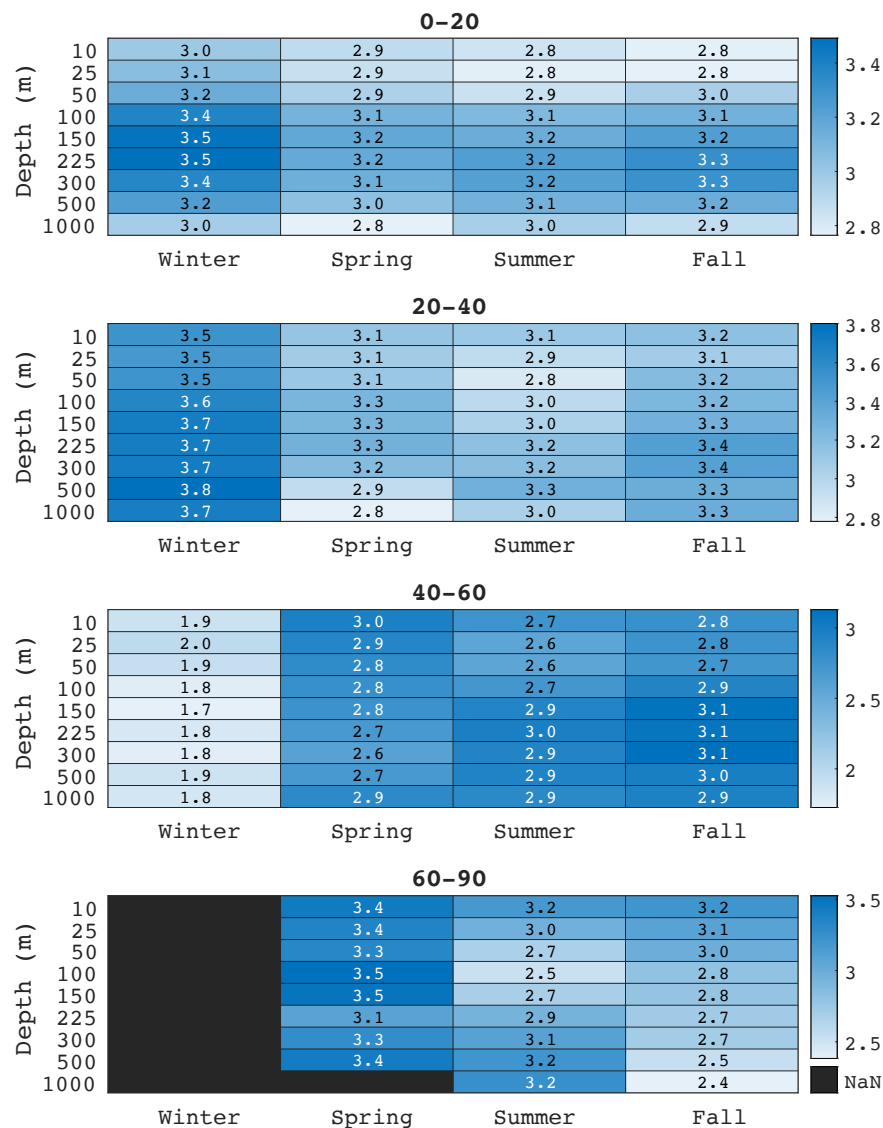
Kiko, R., Bianchi, D., Grenz, C., Hauss, H., Iversen, M., Kumar, S., ... & Robinson, C. (2020). Zooplankton and Nekton: Gatekeepers of the Biological Pump. *Frontiers in Marine Science*, 7, 545.

Kiko, Rainer; Picheral, Marc; Antoine, David; Babin, Marcel; Berline, Leo; Biard, Tristan; Boss, Emmanuel; Brandt, Peter; Carlotti, F; Christiansen, Svenja; Coppola, Laurent; de la Cruz, Leandro; Diamond-Riquier, Emilie; de Madron, Xavier Durrieu; Elineau, Amanda; Gorsky, Gabriel; Guidi, Lionel; Hauss, Helena; Irisson, Jean-Olivier; Karp-Boss, Lee; Karstensen, Johannes; Kim, Dong-gyun; Lekanoff, Rachel M; Lombard, Fabien; Lopes, Rubens M; Marec, Claudie; McDonnell, Andrew; Niemeyer, Daniela; Noyon, Margaux; O'Daly, Stephanie; Ohman, Mark; Pretty, Jessica L; Rogge, Andreas; Searson, Sarah; Shibata, Masashi; Tanaka, Yuji; Tanhua, Toste; Taucher, Jan; Trudnowska, Emilia; Turner, Jessie S; Waite, Anya M; Stemmann, Lars (2021): The global marine particle size distribution dataset obtained with the Underwater Vision Profiler 5 - version 1. PANGAEA <https://doi.pangaea.de/10.1594/PANGAEA.924375>

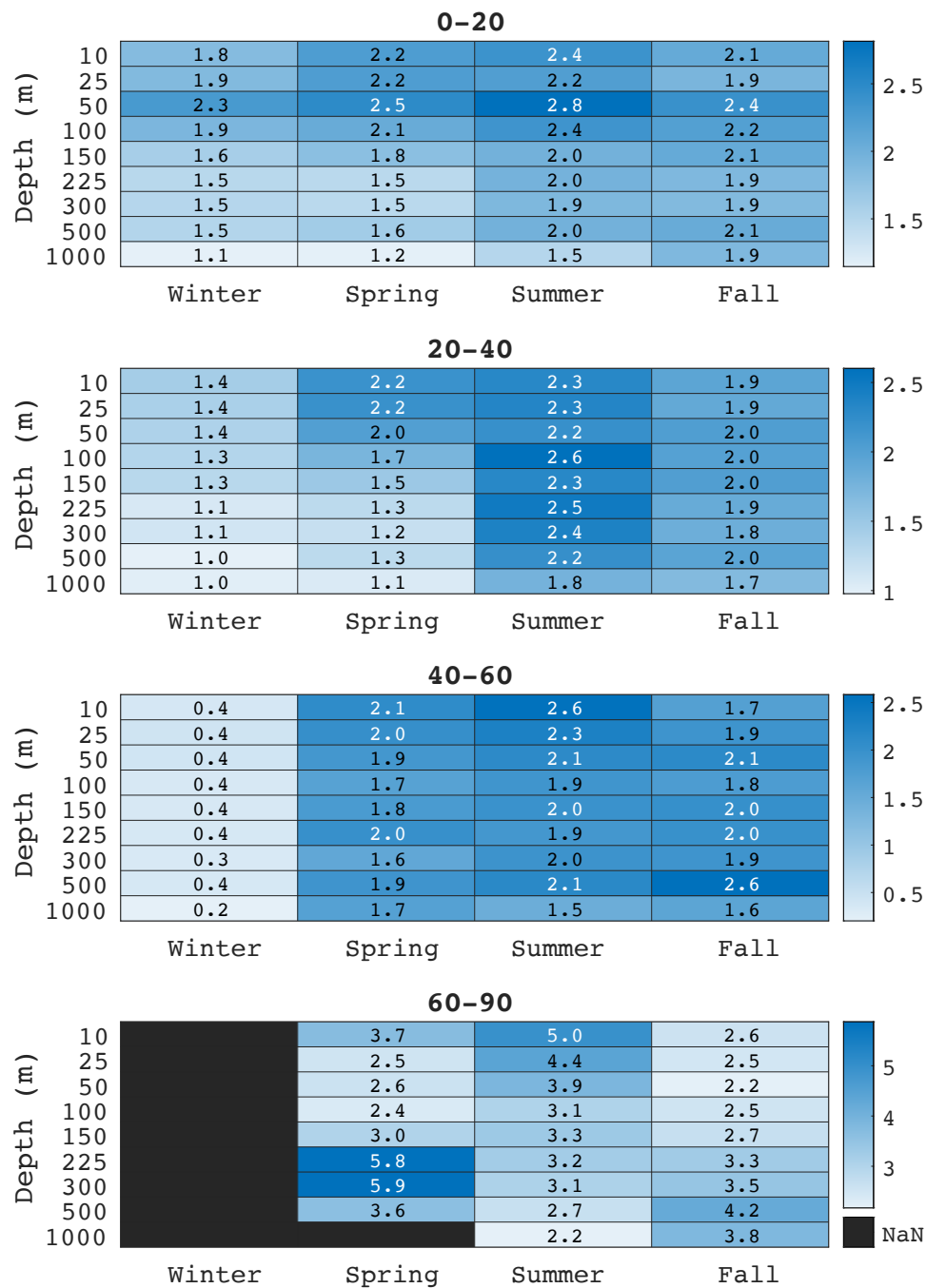


- Kiko, R., Biastoch, A., Brandt, P., Cravatte, S., Hauss, H., Hummels, R., ... & Stemmann, L. (2017). Biological and physical influences on marine snowfall at the equator. *Nature Geoscience*, 10(11), 852-858.
- Kriest, I. (2002). Different parameterizations of marine snow in a 1D-model and their influence on representation of marine snow, nitrogen budget and sedimentation. *Deep Sea Research Part I: Oceanographic Research Papers*, 49(12), 2133-2162.
- Lombard, F., Boss, E., Waite, A. M., Vogt, M., Uitz, J., Stemmann, L., ... & Appeltans, W. (2019). Globally consistent quantitative observations of planktonic ecosystems. *Frontiers in Marine Science*, 6, 196.
- Lunn, D., Jackson, C., Best, N., Thomas, A., & Spiegelhalter, D. (2012). The BUGS Book: A Practical Introduction to Bayesian Analysis (CRC, Boca Raton, FL).
- Michaels, A. F., & Silver, M. W. (1988). Primary production, sinking fluxes and the microbial food web. *Deep Sea Research Part A. Oceanographic Research Papers*, 35(4), 473-490.
- Picheral, M., Guidi, L., Stemmann, L., Karl, D. M., Iddaoud, G., & Gorsky, G. (2010). The Underwater Vision Profiler 5: An advanced instrument for high spatial resolution studies of particle size spectra and zooplankton. *Limnology and Oceanography: Methods*, 8(9), 462-473.
- Reynolds, R. A., Stramski, D., Wright, V. M., & Woźniak, S. B. (2010). Measurements and characterization of particle size distributions in coastal waters. *Journal of Geophysical Research: Oceans*, 115(C8).
- Siegel, D. A., Buesseler, K. O., Doney, S. C., Sailley, S. F., Behrenfeld, M. J., & Boyd, P. W. (2014). Global assessment of ocean carbon export by combining satellite observations and food-web models. *Global Biogeochemical Cycles*, 28(3), 181-196.

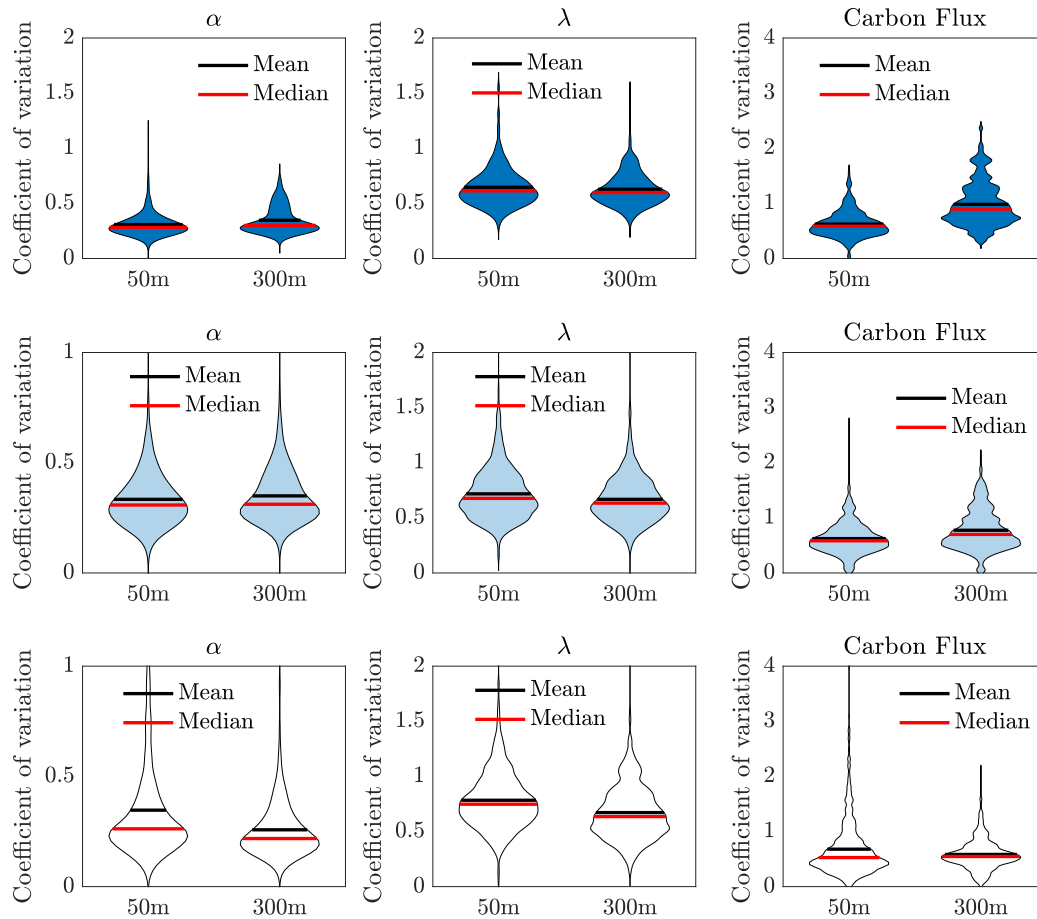
- Sheldon, R. W., Prakash, A., & Sutcliffe Jr, W. (1972). The size distribution of particles in the Ocean 1. *Limnology and oceanography*, 17(3), 327-340.
- Slade, W. H., & Boss, E. (2015). Spectral attenuation and backscattering as indicators of average particle size. *Applied optics*, 54(24), 7264-7277.
- Stemmann, L., & Boss, E. (2012). Plankton and particle size and packaging: from determining optical properties to driving the biological pump. *Annual Review of Marine Science*, 4, 263-290.
- Thomsen, S., Karstensen, J., Kiko, R., Krahmann, G., Dengler, M., & Engel, A. (2019). Remote and local drivers of oxygen and nitrate variability in the shallow oxygen minimum zone off Mauritania in June 2014. *Biogeosciences*, 16(5), 979-998.
- White, A. E., Letelier, R. M., Whitmire, A. L., Barone, B., Bidigare, R. R., Church, M. J., & Karl, D. M. (2015). Phenology of particle size distributions and primary productivity in the North Pacific subtropical gyre (Station ALOHA). *Journal of Geophysical Research: Oceans*, 120(11), 7381-7399.



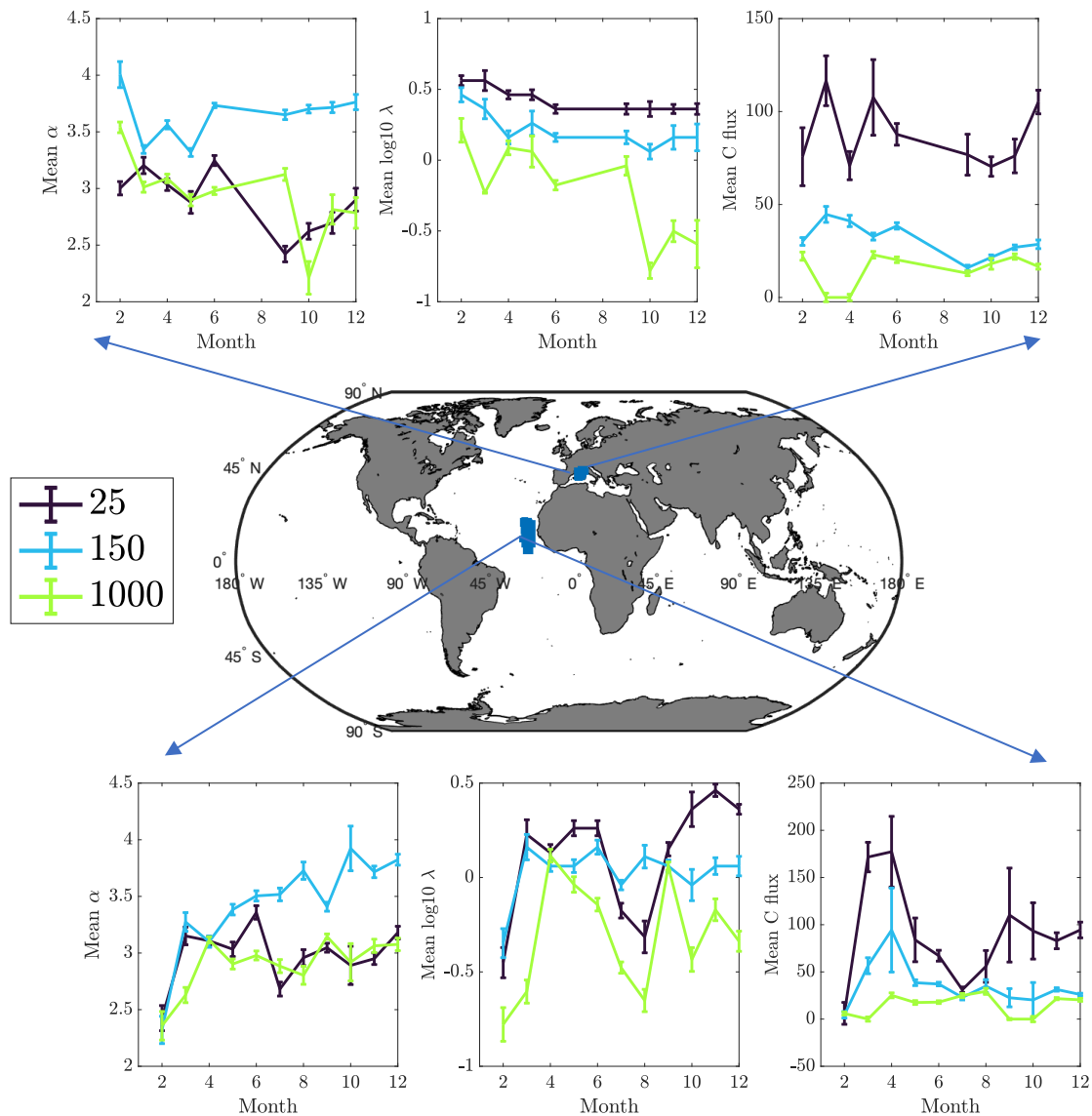
Supplementary Figure 1. Average values of alpha based on season, and at specific latitudinal bands with depth. Note that 0-20 means -20 to 0 and 0 – 20.



Supplementary Figure 2. Average values of  $\lambda$  (normalized to  $\lambda_0 = 1$  mm) based on season, and at specific latitudinal bands with depth. Note that 0-20 means 20S to 0 and 0 – 20N. Note average values of lambda were performed on  $\log_{10}(\lambda)$  and are converted back to non  $\log_{10}$  transformed values.

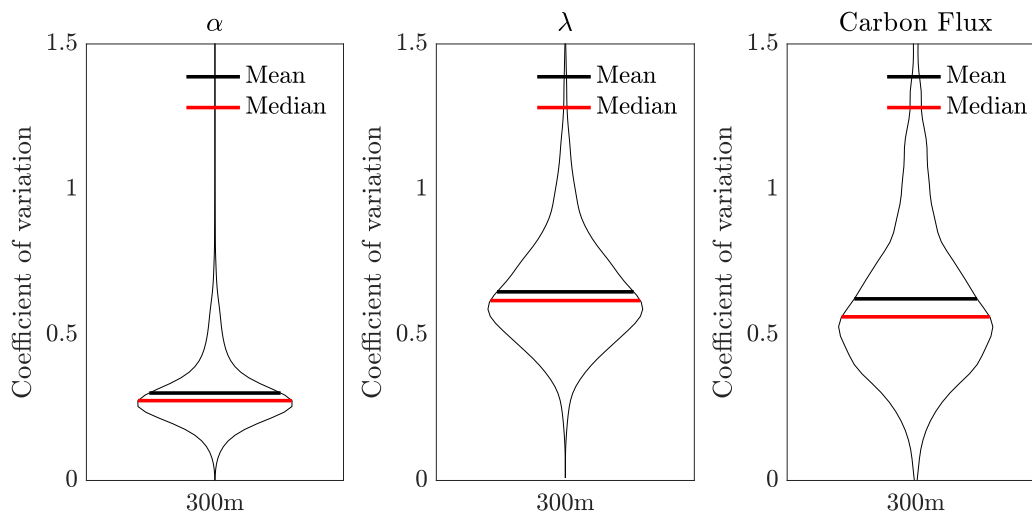


Supplementary Figure 3. Violin plots for coefficient of variation in  $\alpha$  (left),  $\lambda$  (middle) and carbon flux based on either 50m or 300m for three locations. The top row (dark blue violins) is the P16 line in the Pacific. The middle row (light blue) is the Mediterranean. The third row (white) is the Arctic.



Supplementary Figure 4. Seasonal transitions of alpha, lambda, and carbon flux (calculated with 'Kiko' parameters,  $\text{mg C m}^{-2} \text{d}^{-1}$ ) at the 2 locations worldwide that have sufficient observations over a 5x5 degree grid annually (i.e., must have at least 100 observations annually and at least 8 months of casts). Error bars represent the standard error for each month at different depths (25m in black, 150m in blue, and 1000m in green).

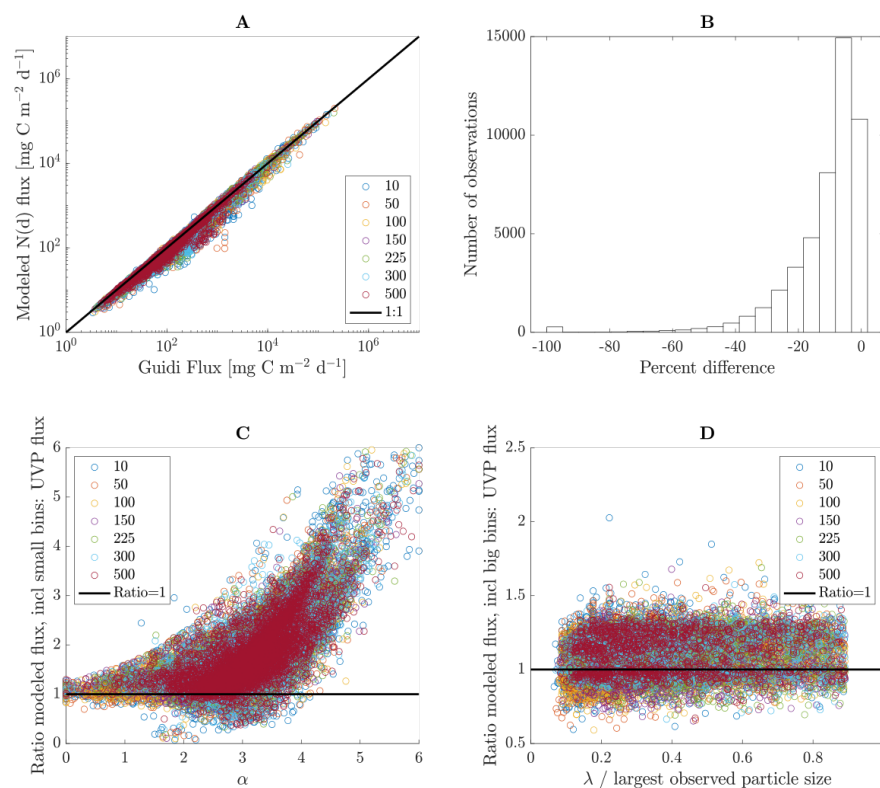
823



824

825

826 Supplementary Figure 5. Violin plots for coefficient of variation in  $\alpha$  (left),  $\lambda$  (middle) and  
 827 carbon flux based on 300m (resulting from the bootstrap procedure where sample volume was  
 828 doubled as a test case). The coefficient of variation reported in this figure is due only to the  
 829 sampling volume uncertainty and not natural spatiotemporal variations worldwide.



830

831 Supplementary Figure 6. A. Flux comparisons between modeled  $N(d)$  flux (y axis) and  $N(d)$  flux  
 832 from UVP observations ('Guidi flux') over the same particle size range. B. Histogram of percent  
 833 difference (relative to 'Guidi flux') between all flux determinations in A. C. The ratio of

modeled  $N(d)$  flux (including 2 size bins smaller than the observed size range) to observed  $N(d)$  flux as a function of depth (colored dots) and  $\alpha$  value. Black line represents equivalent fluxes.  
D. The ratio of modeled  $N(d)$  flux (including 2 size bins larger than the observed size range) to observed  $N(d)$  flux as a function of depth (colored dots) and  $\lambda$  value relative to largest observed particle size. Black line represents equivalent fluxes.